arXiv:2112.01969v8 [cond-mat.stat-mech] 10 May 2022

Experimental Observations of the Effects of Intermolecular Van der Waals Forces on Entropy

Matthew David Marko

Marko Motors LLC

Seaside Heights, NJ, USA

mattdmarko@gmail.com

2 May 2022

Published in Nature Scientific Reports, **12**, 7105, 2 May 2022.

http://doi.org/10.1038/s41598-022-11093-z

Abstract

An experimental effort was conducted to measure the change in internal energy of non-ideal carbon dioxide as its volume rapidly expanded with the sudden opening of a valve from one to two compressed gas cylinders. This was achieved by measuring the mass heat capacity of the gas cylinders and the manifold-valve, and measuring the change in temperature from the sudden doubling of volume of the non-ideal carbon dioxide. It was determined that an empirical equation for the change in internal energy of a non-ideal fluid was more accurate than previous methods used for estimating the change in internal energy by estimating the change in entropy. With this empirical equation, a theoretical ideal Stirling cycle heat engine that exceeds the Carnot efficiency was realized by utilizing non-ideal carbon dioxide as a working fluid.

1 Introduction

In an earlier publication [1], a theoretical Stirling cycle heat engine utilizing a real working fluid with significant intermolecular attractive (and repulsive) Van der Waals forces [2–22] was proposed. The intermolecular attractive Van der Waals forces would both decrease the required work input during the cold isothermal compression, as well as reduce the work output recovered during the hot isothermal expansion. If one were to look at empirical equations of state for real fluids, such as Redlich-Kwong [23] and Peng-Robinson [24], it becomes clear that the intermolecular attractive force increases with decreasing temperatures. Because of the temperature dependence of the Van der Waals forces, which increase in strength with decreasing temperature, the reduction in cold work input is greater than the loss of the hot work output; therefore, the ideal efficiency of this macroscopic heat engine could in theory exceed the Carnot efficiency η_C

$$\eta_C = 1 - \frac{T_L}{T_H}. \tag{1}$$

Originally there were measurements of the enthalpy of vaporization of water [25, 26]; when calculating for the change in internal energy during vaporization, which is isothermal expansion of a real fluid, it was observed that the change in specific internal energy $\delta u_{\delta T=0}$ (J/kg) during isothermal compression and expansion followed a distinct empirical equation

$$\begin{aligned} \delta u_{\delta T=0} &= a' \cdot T^{-0.25} \cdot (\rho_1 - \rho_2), \\ a' &= \frac{0.21836}{9 \cdot (2^{\frac{1}{3}} - 1)} \cdot \frac{R_G^2 \cdot T_C^{2.5}}{P_C}. \end{aligned} \tag{2}$$

where ρ_1 and ρ_2 (m^3/kg) represent the density, T (K) represents the absolute temperature, R_G (J/kg·K) represents the gas constant, T_C (K) represents the critical temperature, and P_C (Pa) represents the critical pressure. This equation has been found to match well for numerous fluids [1, 25–50].

For non-isothermal changes in specific internal energy of a fluid δu (J/kg), one must

include the specific intermolecular kinetic energy $u_{KE} = C_V \cdot R_G \cdot T$ (J/kg) [51],

$$\begin{aligned} \delta u &= C_V \cdot R_G \cdot \delta T - a' \cdot T^{-0.25} \cdot \delta \rho, \\ a' &= \frac{0.21836}{9 \cdot (2^{\frac{1}{3}} - 1)} \cdot \frac{R_G^2 \cdot T_C^{2.5}}{P_C}. \end{aligned} \tag{3}$$

where T (K) represents the absolute temperature, R_G (J/kg·K) represents the gas constant, and C_V is equal to the number of degrees of freedom of the molecule plus one half (ex. monatomic fluids $C_V = 1.5$, diatomic fluids $C_V = 2.5$, etc). By integrating equation 3 from a given density ρ (kg/m^3) to infinitely low density (a true ideal gas) to find the intermolecular potential energy, and the temperature from absolute zero to the current temperature T, one can calculate the total specific internal energy u (J/kg) with equation 4

$$\begin{aligned} u &= C_V \cdot R_G \cdot T - a' \cdot \rho \cdot T^{-0.25}, \\ a' &= \frac{0.21836}{9 \cdot (2^{\frac{1}{3}} - 1)} \cdot \frac{R_G^2 \cdot T_C^{2.5}}{P_C}. \end{aligned} \tag{4}$$

Clausius' Theorem for the second law [2]

$$\oint \frac{\delta q}{T} \leq 0, \tag{5}$$

states that any internally reversible thermodynamic cycle must generate a positive entropy $\delta s_u \geq 0$ to the surrounding universe, where the change in specific entropy δs (J/kg·K) is defined as [3–7]

$$\delta s = \frac{\delta q}{T}, \tag{6}$$

where T (K) is the absolute temperature, and δq (J/kg) represent the heat transferred per unit mass. If a fluid were to consistently follow equation 5, then the change in specific internal energy δu (J/kg) would consistently follow equation 7 [1,3,4,6]

$$\delta u = C_V \cdot R_G \delta T + \{T \cdot (\frac{\partial P}{\partial T})_V - P\} \cdot \delta v. \tag{7}$$

It should be noted that in most of the experimental measurements of the enthalpy of vaporization [1, 25–50] there is great similarity between equation 3 and equation 7.

Clausius' equation 5 makes intuitive sense for a reversible thermodynamic process utilizing an ideal-gas as its working fluid. With a real-fluid, however, intermolecular Van-der-Waals forces impact the molecular behavior and thermodynamic properties. In most published references and tables, the specific internal energy u (J/kg) is often set to zero at an arbitrary point (often the triple-point), and calculated assuming equation 7, which was formulated for the purpose of holding equation 5 applicable.

In contrast, equation 3 is an empirical equation based on measurements of the change in internal energy for numerous different molecules during vaporization. In addition, equation 3 makes physical sense, as it includes both the internal kinetic energy of the molecules as defined with the Kinetic Gas Theory [51], as well as the intermolecular potential energy. Lennard-Jones [6, 52, 53], a well-established approximation for the potential energy from intermolecular attractive and repulsive Van der Waals forces, assumes the attractive force is inverse proportional to the molecular distance to the sixth power r^{-6} (m^{-6}); the attractive intermolecular force is thus inverse proportion to the specific volume squared v^{-2} (m^{-6}), and this is observed in most empirical equations of state for a real fluid [23, 24]. Integrating a potential force inverse-proportional to the specific volume squared would yield a potential energy inverse proportional to the specific volume v (m^3/kg), or proportional to the density ρ (kg/m^3), as observed in equations 3 and 4.

$$\int_v^\infty \frac{\delta v_0}{v_0^2} = \frac{1}{v} = \rho.$$

2 Non-Ideal Stirling Cycle Heat Engine

A Stirling cycle heat engine [1, 4] has isothermal (constant temperature) compression at a cold sink (Stage 1-2), isochoric (constant volume) heating to a hot temperature (Stage 2-3), isothermal expansion at the hot temperature source (Stage 3-4), and isochoric cooling back to the cold temperature (Stage 4-1). For a true, ideal-gas Stirling engine to reach the Carnot

efficiency (equation 1), it is necessary for all of the heat output from the isochoric cooling to go to the isochoric heating.

As a demonstration, carbon dioxide will be the working fluid, with a cold temperature of 32°C and a hot temperature of 82°C. The density will shift from 70 kg/m^3 to 700 kg/m^3. Using equation 1, the Carnot efficiency η_C

$$\eta_C = 1 - \frac{32 + 273.15}{82 + 273.15} = 14.08\%.$$

The thermodynamic properties of this Stirling cycle engine are tabulated in Table 1, using both equation 4 for the specific internal energy u (J/kg) and the National Institute of Standards and Technology (NIST) Chemistry WebBook [54]. The pressures used to calculate the specific work inputs and outputs $w = \int P \cdot \delta v$ (J/kg) from NIST [54] are tabulated in Table 2. The efficiency is calculated as

$$\eta \quad = \quad -\frac{w_{12} + w_{34}}{q_{23} + q_{34} + q_{41}}. \tag{8}$$

If the Stirling engine is utilizing an ideal-gas, then inherently $q_{23} = -q_{41}$; with a real fluid $q_{23} > -q_{41}$, and thus these values need to be included in equation 8.

The efficiency η calculated with the values from NIST [54], derived with equation 7, is 13.92%,

$$\eta_{NIST} = -\frac{w_{12} + w_{34}}{q_{23} + q_{34} + q_{41}} = -\frac{69,149 - 105,515}{47,000 + 252,155 - 37,850} = \frac{36,367}{261,305} = 13.92\%.$$

The efficiency calculated with equation 4 is 16.89%,

$$\eta_{calc} = -\frac{w_{12} + w_{34}}{q_{23} + q_{34} + q_{41}} = -\frac{69,149 - 105,515}{37,603 + 211,232 - 33,516} = \frac{36,367}{215,319} = 16.89\%,$$

which actually exceeds the Carnot efficiency η_C of 14.08%!

If one calculates the change in entropy δs (J/kg·°C) to the ambient universe with equa-

tion 6 throughout the full cycle

$$\delta s_{NIST} = \oint \frac{\delta q}{T} = (\frac{q_{23} + q_{34} + q_{41}}{T_H} + \frac{q_{12}}{T_L}) = (\frac{261,305}{82 + 273.15} + \frac{-224,939}{32 + 273.15}) = -1.38,$$
$$\delta s_{calc} = \oint \frac{\delta q}{T} = (\frac{q_{23} + q_{34} + q_{41}}{T_H} + \frac{q_{12}}{T_L}) = (\frac{215,319}{82 + 273.15} + \frac{-178,953}{32 + 273.15}) = 19.83,$$

it is noticed that the net total change in entropy per cycle with the NIST [54] internal energies δs_{NIST} (J/kg·°C), derived with equation 7, obeys Clausius' equation 5; equation 7 was in fact originally derived to ensure a thermodynamic cycle obeys Clausius' equation 5. If one assumes the internal energy of a real fluid can be determined with equation 4, an empirical equation based on previous measurements of the enthalpy of vaporization [1,25–50] then the net total change in entropy per cycle δs_{calc} (J/kg·°C) fails to obey Clausius' equation 5.

If the theoretical macroscopic Stirling cycle heat engine utilizing real fluids described is to exceed the Carnot efficiency, then equation 3 must be the most accurate description of the change in internal energy for a non-ideal fluid. If Clausius' (equation 5) remains applicable in the presence of intermolecular Van der Waals forces, however, then equation 7 would apply; inherently equation 7 would have greater changes in internal potential energy during isothermal compression and expansion of a real fluid (observed in Table 1), and ensuring the ideal Stirling efficiency η is less than or equal to the Carnot efficiency η_C defined in equation 1. It is thus desired to perform an experiment to determine which, equation 3 or equation 7, is the most accurate definition of the change in specific internal energy δu (J/kg) of a non-ideal fluid.

3 Experimental Description

To determine if equation 3 or equation 7 is the most accurate definition of δu (J/kg), a simple and easily repeatable experiment was performed. Two compressed gas cylinders, manufactured by *Luxfur*, with a volume of 3.4 liters each, and designed to hold 5 lbs of carbon dioxide (CO_2), were obtained. They were connected by a manifold assembly (Figure 1) which included adapters from the CGA-320 valve to NPT, a ball valve, a tee, and a

separate ball valve (to bleed the small amount of CO_2 during disassembly). Three calibrated thermocouples (Taylor # 9940, Panel-Mount LCD Thermometer with Remote Probe; range -40°C to 150°C) were used, with one attached via aluminum tape to each cylinder, and the third attached to the manifold.

Before the experiment could commence, it was necessary to characterize the mass heat capacity mC_P (J/°C) of both the individual cylinders, as well as the manifold assembly. First, the cylinder or manifold was left in a freezer (maintained at a temperature of -20°C) for at least 24 hours, and the temperature inside the freezer was first measured and recorded as $T_{0,Sample}$ (°C). A mass (kg) of water was first weighed, and this water was poured into a bag resting inside an insulated chest. A thermocouple was left in the bottom of the bag, and the temperature was then collected as the initial temperature of the water $T_{0,Water}$ (°C). The sample, either the cylinder or the manifold, was quickly moved into the water-filled bag, and insulating material was then piled on top of the bag to the limit that the insulated chest could be securely closed. The water temperature, measured by the thermocouple, would quickly drop and later settle. It was observed that the temperature would often settle after 15 minutes, but the final temperature T_F (°C) was collected after 60 minutes (minimal difference between the 15 minute measurements). By using the NIST Chemistry WebBook [54] to determine the heat Q_{water} (J) out of the mass of water from the change in temperature, the heat into the sample could be determined, and the mass heat capacity mC_P (J/°C) could be estimated

$$mC_P = \frac{Q_{water}}{T_F - T_{0,Sample}}. \tag{9}$$

This was performed twice with both the cylinder and the manifold, and the results are tabulated in Table 3. The averaged measured mass heat capacity of the cylinder is 2,524 J/°C, and the mass heat capacity of the manifold is 454 J/°C.

The process of the experiment was to have a mass of CO_2 in Cylinder 1, and leave Cylinder 2 empty. The mass of CO_2 was determined by simply weighing Cylinder 1 before the experiment, and subtracting the measured mass of the empty cylinder (3,460.6 g). The

initial temperature on Cylinder 1, Cylinder 2, and the manifold (3) was recorded, and then the two-cylinder assembly was added to the insulated chest and thoroughly covered in insulation (Figure 2). To commence the experiment, the ball valve was suddenly opened, allowing for CO_2 to flow from Cylinder 1 to Cylinder 2, thus instantly doubling the volume and suddenly dropping the temperature due to the Joule–Thomson effect [55]. Over time, the temperature of the cylinders and manifold would drop, as heat would flow from the aluminum cylinders and steel manifold into the cooler CO_2 until they reached thermal equilibrium, and the final temperature on Cylinder 1, Cylinder 2, and the manifold (3) was recorded. The results of these temperature measurements are tabulated in Table 4.

Afterwards, the remaining mass of CO_2 in Cylinder 1 and Cylinder 2 was recorded, and these results, along with the initial mass in Cylinder 1, are tabulated in Table 5. In addition, with the known temperatures (Table 4) and densities (mass over the 3.4 liter volume), the specific internal energy u (kJ/kg) values as determined by the NIST Chemistry WebBook [54] (which were derived by NIST with equation 7) were collected and tabulated in Table 5. On average, less than 1% of the CO_2 was lost in the disassembly of the manifold or due to leaking. In addition, it was frequently observed that only a small portion of the mass (approximately 400g) would travel from Cylinder 1 to Cylinder 2; this is expected, as much of the liquid CO_2 (and thus most of the mass) would stay in the original Cylinder 1 rather than travel through the manifold. It was also noticed that at times Cylinder 2 would experience a slight *increase* in temperature; mainly due to the kinetic energy of expansion, and the low masses of CO_2 that made its way into Cylinder 2.

4 Experimental Analysis

Carbon dioxide (CO_2) [56] has a critical temperature T_C of 304.128 K; a critical pressure P_C of 7,377,300 Pa; a critical specific density ρ_C of 467.6 (kg/m^3), 3 degrees of freedom, a molar mass of 44 g/mole, and a Pitzer eccentric factor [57] of 0.228. The specific gas constant R_G for CO_2 is 188.924 J/kg·°C; the ideal-gas specific heat at a constant volume $C_V = 3.5 \cdot R_G$; and the specific heat ratio $\kappa = \frac{C_P}{C_V} = \frac{4.5}{3.5} = 1.28$. For CO_2, the value of *a'* as

defined in equation 4 is 728.46 $Pa{\cdot}K^{0.25}{\cdot}m^6{\cdot}kg^{-2}$.

The density of saturated liquid CO_2 ρ_L (kg/m^3) and saturated gas CO_2 ρ_G (kg/m^3) is defined with equation 10 [56]

$$\begin{aligned} ln(\frac{\rho_L}{\rho_C}) &= \Sigma_{i=1}^{4} a_i{\cdot}(1-\frac{T}{T_C})^{t_i}, \\ ln(\frac{\rho_G}{\rho_C}) &= \Sigma_{i=1}^{5} b_i{\cdot}(1-\frac{T}{T_C})^{u_i}, \end{aligned} \tag{10}$$

where T_C is 304.128 K, ρ_C is 467.6 (kg/m^3), and the values of a_i, t_i, b_i, and u_i are tabulated in Table 6.

Table 7 contains the tabulated densities ρ (kg/m^3) of the CO_2, both before the experiment ρ_0 (kg/m^3), and after the experiment in Cylinder 1 ρ_{F1} (kg/m^3) and Cylinder 2 ρ_{F2} (kg/m^3). In addition, the densities of a saturated liquid ρ_L (kg/m^3) and a saturated gas ρ_G (kg/m^3) for the experimentally measured CO_2 temperatures (Table 4) as determined with equation 10 is also tabulated in Table 7. With the density ρ (kg/m^3), saturated liquid density ρ_L (kg/m^3), and saturated gas density ρ_G (kg/m^3), the vapor quality X was determined with equation 11, and tabulated in Table 8.

$$X = \frac{(1/\rho)-(1/\rho_L)}{(1/\rho_G)-(1/\rho_L)} = \frac{v-v_L}{v_G-v_L}. \tag{11}$$

Utilizing the density ρ (kg/m^3), saturated liquid density ρ_L (kg/m^3), and saturated gas density ρ_G (kg/m^3) tabulated in Table 7, as well as the experimentally measured temperatures tabulated in Table 4, and the masses of CO_2 tabulated in Table 5, the internal energy U (kJ) was calculated using the empirical equation 4, and tabulated in Table 9.

For qualities X greater than 1, the CO_2 is treated as a vapor, and the internal energy is estimated solely with the empirical equation 4, and the final internal energy U (kJ) was tabulated in Table 10. For qualities X less than 1 (there were no measurements at a greater density than the saturated liquid density), the internal energy of the liquid-vapor mixture U (kJ) was calculated with equation 12 from the quality X (Table 11), saturated liquid internal energy U_L (kJ), and the saturated gas internal energy U_G (kJ), both tabulated in

Table 9.

$$U = U_L \cdot (1 - X) + U_G \cdot X. \quad (12)$$

All of these final internal energies U (kJ) are tabulated in Table 10.

Finally, the estimated heat inputs were determined with equation 13, plotted in Figure 3, and tabulated in Table 11. These include the heat estimates Q_{theory} (kJ) utilizing the internal energies derived from the empirical equation 4 and tabulated in Table 10; as well as the heat estimates Q_{NIST} (kJ) utilizing the specific internal energies collected from the NIST Chemistry WebBook [54] and tabulated in Table 5.

$$Q = U_{F1} + U_{F2} - U_0. \quad (13)$$

The values of Q_{theory} (kJ) and Q_{NIST} (kJ) are compared to the experimentally measured heat inputs Q_{EXP} (kJ), determined by comparing the measured changes in temperature (Table 4) with the mass heat capacity tabulated in Table 3, as described in equation 14,

$$Q_{EXP} = mC_{P,Cylinder} \cdot (T_{1,0} + T_{2,0} - T_{1,F} - T_{2,F}) + mC_{P,Manifold} \cdot (T_{3,0} - T_{3,F}). \quad (14)$$

5 Conclusion

When analyzing the results of Table 11 and Figure 3, with 25 independent test results, the correlation between Q_{Theory} (equation 3) and Q_{EXP} is 0.9560; in excess of the correlation of 0.9229 between Q_{NIST} (equation 7) and Q_{EXP}. The average error between Q_{Theory} and Q_{EXP} is 29%, less than the average error of 64% between Q_{NIST} and Q_{EXP}. The median error between Q_{Theory} and Q_{EXP} is 17%, less than the median error of 27% between Q_{NIST} and Q_{EXP}. Finally, the standard deviation of the error between Q_{Theory} and Q_{EXP} is 29%, less than the standard deviation of the error of 153% between Q_{NIST} and Q_{EXP}. The experimental data suggests that equation 3 is the most accurate definition of the change in internal energy of a real fluid δu (J/kg), as compared to equation 7. This effort provides

an experimental justification to the possibility of the theoretical macroscopic Stirling cycle heat engine utilizing real fluids described earlier [1] exceeding the Carnot efficiency.

Data availability

All data generated or analysed during this study are included in this published article [and its supplementary information files].

Stage	P (Pa)	T (K)	ρ (kg/m^3)	u_{NIST} (J/kg)	u_{calc} (J/kg)
1	3,334,500	305.15	70	430,810	189,575
2	8,650,400	305.15	700	275,020	79,771
3	26,745,000	355.15	700	322,020	117,374
4	4,132,200	355.15	70	468,660	223,091
Stages	w (J/kg)	δu_{NIST} (J/kg)	q_{NIST} (J/kg)	δu_{calc} (J/kg)	q_{calc} (J/kg)
12	69,149	-155,790	-224,939	-109,804	-178,953
23	0	47,000	47,000	37,603	37,603
34	-105,515	146,640	252,155	105,717	211,232
41	0	-37,850	-37,850	-33,516	-33,516

Table 1: The stages of the non-ideal Stirling cycle heat engine, as well as the specific work inputs and outputs w (J/kg), specific heat inputs and outputs q (J/kg), and specific internal energies u (J/kg) from both *NIST* [54] and calculated *calc* with equation 4.

ρ (kg/m^3)	P_L (MPa)	P_H (MPa)	u_L (kJ/kg)	u_H (kJ/kg)
70	3.3345	4.1322	430.81	468.66
88.146	3.5471	5.0367	428.9	463.45
107.63	3.7598	5.9412	426.92	457.93
128.64	3.9724	6.8457	424.86	452.08
151.42	4.185	7.7502	422.73	445.85
176.22	4.3977	8.6548	420.5	439.22
203.31	4.6103	9.5593	418.18	432.14
232.93	4.823	10.464	415.74	424.59
265.24	5.0356	11.368	413.18	416.58
300.17	5.2482	12.273	410.47	408.18
337.28	5.4609	13.177	407.6	399.53
375.61	5.6735	14.082	404.52	390.85
413.83	5.8861	14.986	401.2	382.42
450.56	6.0988	15.891	397.59	374.49
484.73	6.3114	16.795	393.6	367.23
515.82	6.524	17.7	389.12	360.69
543.76	6.7367	18.604	383.94	354.85
568.77	6.9493	19.509	377.72	349.63
591.17	7.1619	20.413	369.68	344.96
611.31	7.3746	21.318	357.28	340.75
629.52	7.5872	22.222	303.52	336.94
646.07	7.7999	23.127	289.34	333.46
661.22	8.0125	24.031	283.9	330.26
675.15	8.2251	24.936	280.23	327.31
688.03	8.4378	25.84	277.38	324.57
700	8.6504	26.745	275.02	322.02

Table 2: The pressures and specific internal energies versus the density ρ, taken from NIST [54], and used to solve the work and heat inputs and outputs listed in Table 1. The pressure P_L (MPa) and specific internal energy u_L (kJ/kg) is at 32°C, and the pressure P_H (MPa) and specific internal energy u_H (kJ/kg) is at 82°C.

Sample	Mass Water (kg)	T_0 *Sample* (°C)	T_0 *Water* (°C)	T_F (°C)	mC_P (J/°C)
Cylinder	4.01	-16.1	23.7	18.4	2575.23
Cylinder	3.9	-16.3	23.2	18	2473.09
Manifold	1.6	-20	24.7	21.8	464.56
Manifold	1.77	-19.3	24.9	22.4	443.96

Table 3: The results of the effort to find the mass heat capacity mC_P (J/°C) of the cylinder and the manifold.

Test Number	$T_{1,0}$ (°C)	$T_{2,0}$ (°C)	$T_{3,0}$ (°C)	$T_{1,F}$ (°C)	$T_{2,F}$ (°C)	$T_{F,3}$ (°C)
1-1	18.4	19.1	19.4	10.7	11.7	13.1
1-2	18.2	18.7	18.3	7.9	19.9	11.8
1-3	17.9	19.3	19.9	6.9	20.3	12.9
1-4	18.4	19.2	18.7	8.4	20.3	12.7
1-5	17.9	18.1	18.6	13.6	19.3	12.4
2-1	15.1	15.6	15.6	7.5	8.2	9.8
2-2	14.7	15.2	16.0	4.8	16.1	8.9
2-3	10.6	14.5	12.9	1.1	15.6	6.9
2-4	14.5	15.5	16.2	3.4	16.7	8.3
2-5	13.5	15.3	16.3	10.2	16.3	12.1
2-6	13.1	13.3	13.2	11.4	14.2	11.6
3-1	10.9	10.0	10.3	3.1	6.6	4.9
3-2	10.2	9.0	9.7	0.7	10.5	4.2
3-3	7.6	8.9	10.2	-1.7	10.2	3.8
3-4	4.7	9.4	8.5	-4.5	10.4	1.7
3-5	11.2	11.5	11.4	0.4	12.7	5.2
3-6	7.2	11.4	9.9	2.2	11.7	4.1
3-7	8.2	11.2	11.0	7.0	12.0	8.6
4-1	10.9	11.8	12.2	4.5	4.8	6.4
4-2	8.0	9.0	9.2	0.8	5.3	3.9
4-3	9.8	11.1	11.0	0.5	11.6	5.1
4-4	9.4	11.2	10.4	-0.1	12.2	4.9
4-5	8.0	11.2	10.9	-1.6	12.0	3.8
4-6	11.3	11.8	12.3	6.2	12.6	8.5
4-7	11.6	12.1	12.2	9.9	13.0	10.6

Table 4: The measured temperature (°C) of Cylinder *1* and Cylinder *2*, as well as the manifold temperature *3*, both before *0* and after F the manifold valve was opened.

Test Number	$mass_0$ (g)	$mass_{F1}$ (g)	$mass_{F2}$ (g)	u_0 (kJ/kg)	u_{F1} (kJ/kg)	u_{F1} (kJ/kg)
1-1	2026.7	1565.6	459.8	256.95	249.92	391.15
1-2	1565.2	1200.2	364.1	272.42	258.99	408.49
1-3	1199.1	848.4	350.8	292.83	285.54	410.19
1-4	847.4	484.4	342.4	332.90	370.17	411.06
1-5	483.8	246.9	236.3	394.34	415.90	421.39
2-1	1880.4	1385.4	491.0	251.91	247.99	366.59
2-2	1385.4	1054.0	332.0	270.20	258.64	408.73
2-3	1053.8	764.2	288.0	278.59	273.67	413.02
2-4	764.0	444.7	305.1	329.22	357.58	412.07
2-5	444.6	225.9	216.4	394.46	415.61	421.24
2-6	226.3	110.9	109.5	417.76	258.16	431.34
3-1	1941.2	1582.5	349.8	238.88	227.90	398.84
3-2	1582.2	1270.0	299.9	247.85	233.03	407.66
3-3	1270.0	995.4	272.2	254.02	241.40	410.48
3-4	995.8	738.6	238.5	262.85	255.59	414.36
3-5	735.7	442.4	283.4	319.53	341.88	411.23
3-6	442.6	197.7	182.7	380.36	412.78	421.50
3-7	197.6	97.2	94.8	417.26	427.74	431.45
4-1	2233.5	1679.9	551.5	232.55	228.77	329.70
4-2	1679.9	1356.8	321.0	238.32	229.54	401.02
4-3	1356.8	1058.5	296.0	256.33	244.19	408.97
4-4	1058.4	773.8	283.2	274.00	267.86	410.85
4-5	773.5	503.8	268.1	299.86	311.51	412.35
4-6	503.6	257.5	244.1	379.36	408.98	415.44
4-7	257.2	128.7	126.6	413.23	426.21	428.62

Table 5: The measured mass (g) of CO_2 in the 3.4 liter cylinders, as well as the specific internal energy u (kJ/kg) collected from the NIST webbook [54].

	1	2	3	4	5
a_i	1.9245108	-0.62385555	-0.32731127	0.39245142	-
t_i	0.340	0.5	(10/6)	(11.6)	-
b_i	-1.7074879	-0.8227467	-4.6008549	-10.111178	-29.742252
u_i	0.340	0.5	1	(7/3)	(14/3)

Table 6: Coefficient values for equation 10.

Test Num	ρ_0 $(\frac{kg}{m^3})$	ρ_{0-L} $(\frac{kg}{m^3})$	ρ_{0-G} $(\frac{kg}{m^3})$	ρ_{F1} $(\frac{kg}{m^3})$	ρ_{F1-L} $(\frac{kg}{m^3})$	ρ_{F1-G} $(\frac{kg}{m^3})$	ρ_{F2} $(\frac{kg}{m^3})$	ρ_{F2-L} $(\frac{kg}{m^3})$	ρ_{F2-G} $(\frac{kg}{m^3})$
1-1	596.09	789.83	182.35	460.47	855.86	138.39	135.22	848.19	143.19
1-2	460.35	791.80	180.96	353.00	876.26	126.02	107.09	774.46	193.42
1-3	352.68	794.72	178.89	249.53	883.22	121.94	103.18	770.16	196.58
1-4	249.24	789.83	182.35	142.47	872.72	128.12	100.71	770.16	196.58
1-5	142.29	794.72	178.89	72.62	832.99	152.94	69.50	780.74	188.86
2-1	553.06	820.32	161.31	407.47	879.06	124.37	144.41	874.14	127.28
2-2	407.47	823.76	159.02	310.00	897.32	113.88	97.65	811.50	167.27
2-3	309.94	856.61	137.92	224.76	920.75	101.12	84.71	815.95	164.25
2-4	224.71	825.47	157.89	130.79	906.39	108.85	89.74	806.04	171.01
2-5	130.76	833.81	152.40	66.44	859.61	136.07	63.65	809.69	168.51
2-6	66.56	837.08	150.29	32.62	850.51	141.72	32.21	828.00	156.21
3-1	570.94	854.34	139.33	465.44	908.30	107.80	102.88	885.27	120.75
3-2	465.35	859.61	136.07	373.53	923.18	99.84	88.21	857.36	137.46
3-3	373.53	878.37	124.78	292.76	937.45	92.52	80.06	859.61	136.07
3-4	292.88	897.98	113.51	217.24	953.40	84.68	70.15	858.11	136.99
3-5	216.38	852.05	140.76	130.12	925.00	98.89	83.35	840.30	148.21
3-6	130.18	881.15	123.15	58.15	913.96	104.74	53.74	848.19	143.19
3-7	58.12	874.14	127.28	28.59	882.53	122.34	27.88	845.85	144.67
4-1	656.91	854.34	139.33	494.09	899.29	112.78	162.21	897.32	113.88
4-2	494.09	875.56	126.44	399.06	922.58	100.16	94.41	894.02	115.74
4-3	399.06	862.58	134.25	311.32	924.40	99.21	87.06	848.97	142.70
4-4	311.29	865.51	132.46	227.59	928.01	97.33	83.29	844.28	145.67
4-5	227.50	875.56	126.44	148.18	936.87	92.81	78.85	845.85	144.67
4-6	148.12	851.28	141.24	75.74	887.99	119.18	71.79	841.10	147.70
4-7	75.65	848.97	142.70	37.85	861.84	134.70	37.24	837.89	149.76

Table 7: The calculated density of CO_2 in the 3.4 liter cylinders, taken from the mass tabulated in Table 5. The densities of a saturated liquid and a saturated gas are defined with equation 10.

Test	X_0	X_{F1}	X_{F2}
1-1	0.0976	0.1656	1.0709
1-2	0.2133	0.2490	2.0746
1-3	0.3641	0.4068	2.2155
1-4	0.6511	0.8820	2.2782
1-5	1.3319	2.3548	3.2654
2-1	0.1183	0.1907	0.8611
2-2	0.2444	0.2754	1.8982
2-3	0.3385	0.3820	2.1758
2-4	0.6323	0.8093	2.1497
2-5	1.2025	2.2451	3.0805
2-6	2.5332	5.0139	5.7458
3-1	0.0967	0.1281	1.2011
3-2	0.1593	0.1784	1.6650
3-3	0.2238	0.2411	1.8312
3-4	0.2989	0.3303	2.1340
3-5	0.5814	0.7313	1.9447
3-6	0.9372	1.9050	3.0028
3-7	2.3928	4.8072	6.0527
4-1	0.0586	0.1176	0.6588
4-2	0.1303	0.1598	1.2595
4-3	0.2141	0.2368	1.7682
4-4	0.3217	0.3606	1.9050
4-5	0.4808	0.5853	2.0069
4-6	0.9443	1.6626	2.2824
4-7	2.0654	4.0326	4.6798

Table 8: The calculated vapor quality solved with equation 11, utilizing the density ρ (kg/m^3), saturated liquid density ρ_L (kg/m^3), and saturated gas density ρ_G (kg/m^3) tabulated in Table 7.

Test Num	U_{0x} (kJ)	U_{0-L} (kJ)	U_{0-G} (kJ)	U_{F1-x} (kJ)	U_{F1-L} (kJ)	U_{F1-G} (kJ)	U_{F2-x} (kJ)	U_{F2-L} (kJ)	U_{F2-G} (kJ)
1-1	177.74	108.52	325.56	165.91	56.05	255.40	75.57	17.45	74.92
1-2	174.49	83.02	251.60	147.67	35.93	196.14	63.69	20.91	58.15
1-3	156.19	62.70	192.94	119.41	23.67	138.68	61.70	20.52	55.93
1-4	126.13	45.37	136.12	77.91	15.00	79.14	60.37	20.03	54.59
1-5	80.97	25.30	77.84	43.64	10.41	40.13	42.80	13.20	37.83
2-1	174.55	85.70	304.78	156.63	40.34	226.43	78.73	15.00	80.23
2-2	163.86	61.86	224.73	135.42	24.98	172.30	57.77	15.91	53.69
2-3	139.75	37.50	171.92	107.84	12.63	124.75	50.68	13.46	46.63
2-4	114.95	33.76	123.98	70.93	9.32	72.67	53.64	15.06	49.26
2-5	73.98	18.64	72.27	39.66	7.85	36.87	38.99	10.47	34.98
2-6	40.17	9.29	36.81	20.22	4.14	18.08	20.18	4.76	17.78
3-1	167.94	70.32	316.61	157.46	32.23	258.59	58.30	9.55	57.18
3-2	165.71	54.96	258.22	145.02	20.02	207.26	51.55	10.61	48.93
3-3	151.34	37.24	207.56	126.37	11.20	162.14	47.13	9.45	44.42
3-4	130.91	23.40	162.78	102.34	4.50	119.95	41.75	8.39	38.92
3-5	110.09	27.13	119.96	69.71	6.72	72.18	49.38	11.38	46.13
3-6	71.79	12.62	72.34	33.94	3.68	32.29	32.67	6.93	29.77
3-7	34.72	6.04	32.29	17.51	2.73	15.89	17.41	3.66	15.44
4-1	159.16	80.91	364.28	160.29	38.82	274.61	85.40	13.07	90.16
4-2	164.64	50.64	274.52	148.83	21.64	221.44	53.70	7.93	52.48
4-3	157.68	45.98	221.50	132.51	16.28	172.72	51.16	11.17	48.24
4-4	139.20	34.98	172.83	108.15	11.02	126.21	49.25	11.06	46.12
4-5	112.49	23.32	126.40	77.07	5.76	82.07	46.80	10.35	43.67
4-6	81.49	18.68	82.10	44.09	6.82	42.10	43.02	9.75	39.73
4-7	44.98	9.71	41.92	23.22	4.39	21.01	23.12	5.17	20.60

Table 9: The calculated internal energy U (kJ), solved with equation 4, utilizing the measured temperature in Table 4, and the densities tabulated in Table 7.

Test Num	U_0 (kJ)	U_{F1} (kJ)	U_{F2} (kJ)
1-1	129.69	89.06	75.57
1-2	118.97	75.82	63.69
1-3	110.12	70.46	61.70
1-4	104.46	71.57	60.37
1-5	80.97	43.64	42.80
2-1	111.61	75.84	71.17
2-2	101.66	65.55	57.77
2-3	83.00	55.46	50.68
2-4	90.81	60.59	53.64
2-5	73.98	39.66	38.99
2-6	40.17	20.22	20.18
3-1	94.15	61.24	58.30
3-2	87.34	53.43	51.55
3-3	75.36	47.59	47.13
3-4	65.07	42.64	41.75
3-5	81.09	54.60	49.38
3-6	68.60	33.94	32.67
3-7	34.72	17.51	17.41
4-1	97.51	66.55	63.85
4-2	79.81	53.57	53.70
4-3	83.56	53.32	51.16
4-4	79.33	52.56	49.25
4-5	72.88	50.42	46.80
4-6	78.57	44.09	43.02
4-7	44.98	23.22	23.12

Table 10: The calculated internal energies U (kJ), solved with equation 4, adjusting for mixed liquid-vapor, using the internals energies U (kJ) tabulated in Table 9, with the qualities X tabulated in Table 8, solved with equation 12.

Test Num	Q_{Theory} (kJ)	Q_{NIST} (kJ)	Q_{EXP} (kJ)
1-1	34.9442 (14.71%)	50.3454 (22.88%)	40.9726
1-2	20.5379 (20.76%)	33.1792 (28.01%)	25.9194
1-3	22.0339 (22.47%)	35.0143 (23.21%)	28.4180
1-4	27.4844 (9.12%)	37.9578 (50.70%)	25.1876
1-5	5.4758 (48.53%)	11.4785 (7.89%)	10.6392
2-1	35.3962 (12.59%)	49.8695 (23.16%)	40.4932
2-2	21.6599 (16.50%)	33.9698 (30.96%)	25.9394
2-3	23.1390 (3.29%)	34.5102 (44.24%)	23.9256
2-4	23.4268 (18.01%)	33.2143 (16.24%)	28.5742
2-5	4.6671 (39.48%)	9.6657 (25.33%)	7.7120
2-6	0.2402 (91.25%)	-18.6774 (780.27%)	2.7456
3-1	25.3884 (17.36%)	36.4521 (18.66%)	30.7204
3-2	17.6409 (22.25%)	26.0571 (14.84%)	22.6890
3-3	19.3648 (16.16%)	29.4168 (27.36%)	23.0976
3-4	19.3141 (18.79%)	25.8576 (8.72%)	23.7840
3-5	22.8826 (15.39%)	32.7121 (20.95%)	27.0452
3-6	-1.9849 (113.69%)	-9.7327 (167.14%)	14.4960
3-7	0.1985 (90.54%)	0.0272 (98.70%)	2.0992
4-1	32.8876 (9.79%)	46.7398 (28.21%)	36.4548
4-2	27.4498 (8.25%)	39.8135 (33.08%)	29.9178
4-3	20.9232 (15.94%)	31.7417 (27.53%)	24.8898
4-4	22.4886 (6.11%)	33.6212 (40.37%)	23.9510
4-5	24.3473 (4.28%)	35.5481 (39.76%)	25.4346
4-6	8.5325 (32.17%)	15.6756 (24.62%)	12.5784
4-7	1.3649 (50.29%)	2.8338 (3.21%)	2.7456

Table 11: The combined energy input Q (kJ) into the CO_2, defined with equation 13 and equation 14, using the theory defined in equation 4, from NIST in Table 5 [54], and measured experimentally. The parentheses represent the percent (%) error with Q_{EXP}. These tabulated results are plotted in Figure 3.



Figure 1: The manifold to connect the two 3.4 liter CO_2 cylinders.

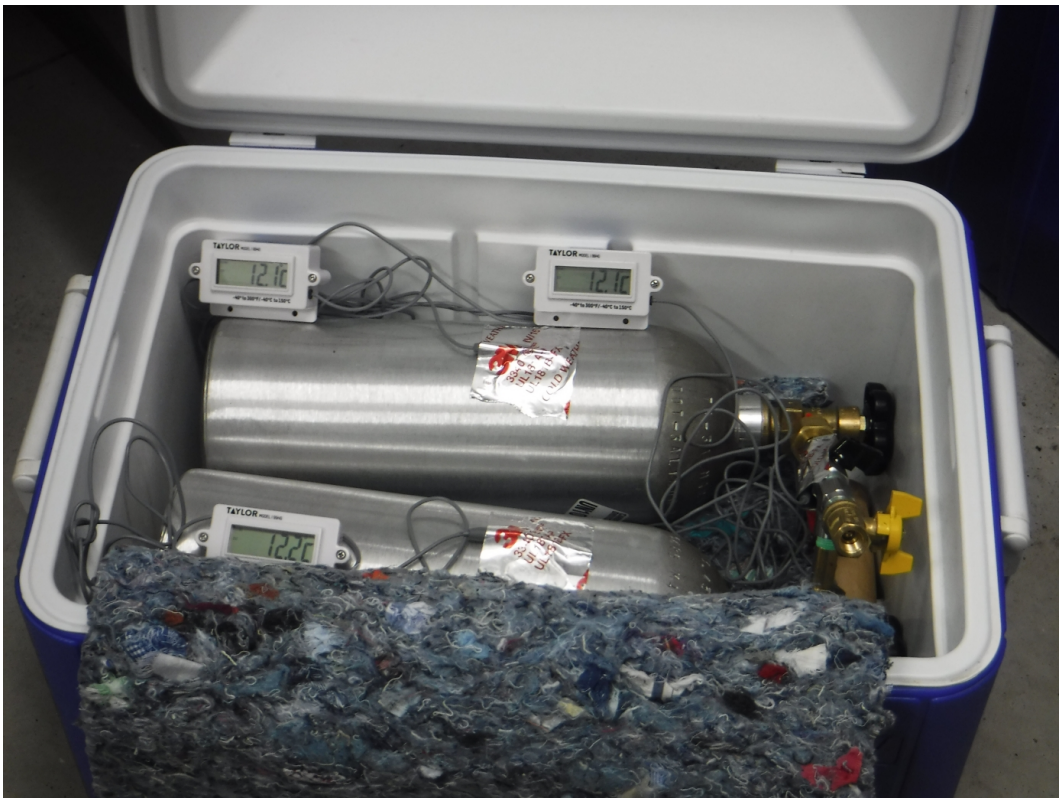


Figure 2: The full experimental apparatus, with two CO_2 cylinders connected by the manifold (Figure 1), inside the insulated chest, with the three thermocouples attached.

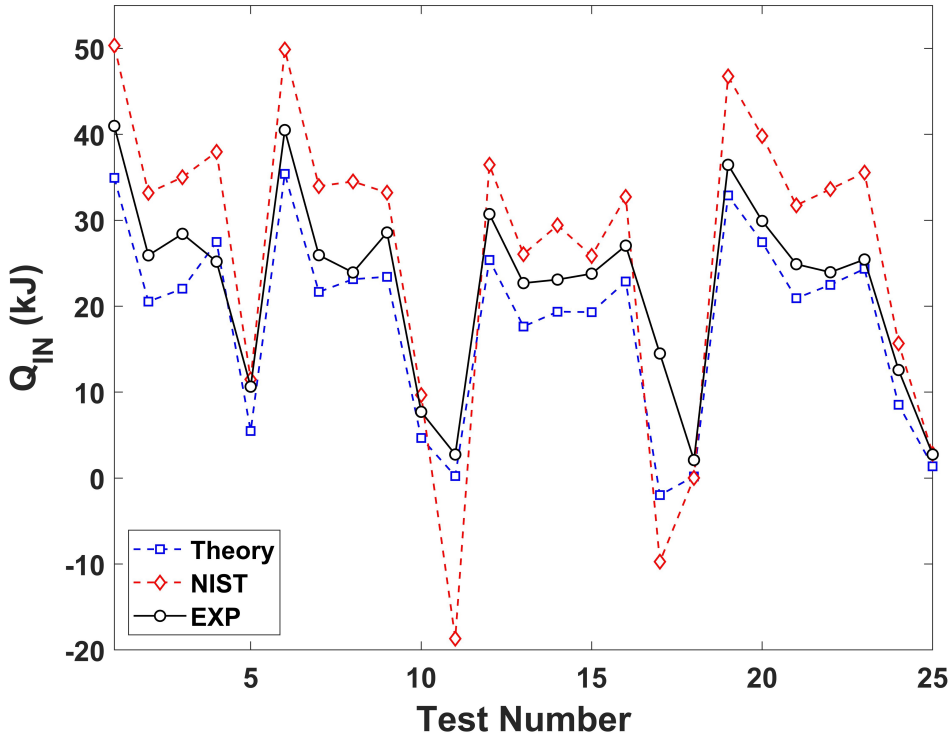


Figure 3: The combined energy input Q (kJ) into the CO_2, defined with equation 13 and equation 14, using the theory defined in equation 4, from NIST in Table 5 [54], and measured experimentally. These plotted results are tabulated in Table 11.

References

[1] Matthew David Marko. The saturated and supercritical stirling cycle thermodynamic heat engine cycle. *AIP Advances*, 8(8):085309, 10 August 2018. https://doi.org/10.1063/1.5043523.

[2] Sadi Carnot, E. Clapeyron, Rudolph Clausius, and E. Mendoza. *Reflections on the Motive Power of Fire and other Papers on the Second Law of Thermodynamics*. Dover Publications Inc, Mineola, NY, 1960.

[3] Enrico Fermi. *Thermodynamics*. Dover Publications Inc, New York, NY, 1936.

[4] Yunus A. Cengel and Michael A. Boles. *Thermodynamics, An Engineering Approach Sixth Edition*. McGraw Hill Higher Education, Columbus OH, 2008.

[5] Daniel V. Schroeder. *An Introduction to Thermal Physics*. Addison Wesley Longman, Boston MA, 2000.

[6] Terrell L. Hill. *An Introduction to Statistical Thermodynamics*. Dover Publications, 1960, 1960.

[7] R. K. Pathria. *Statistical Mechanics, 2nd Edition*. Butterworth-Heinemann, 30 Corporate Drive, Suite 400, Burlington, MA 01803 USA, 1972.

[8] Fabio L. Leite, Carolina C. Bueno, Alessandra L. Da Róz, Ervino C. Ziemath, and Osvaldo N. Oliveira Jr. Theoretical models for surface forces and adhesion and their measurement using atomic force microscopy. *MDPI Molecular Sciences*, 13:12773–12856, 2012. https://doi.org/10.3390/ijms131012773.

[9] W.H. Keesom. The second viral coefficient for rigid spherical molecules, whose mutual attraction is equivalent to that of a quadruplet placed at their centre. *Royal Netherlands Academy of Arts and Sciences Proceedings*, 18 I:636–646, 1915.

[10] The General Theory of Molecular Forces. F. london. *Transactions of the Faraday Society*, 33:8–26, 1937. https://doi.org/10.1039/TF937330008B.

[11] Roger H. French. Origins and applications of london dispersion forces and hamaker constants in ceramics. *Journal of the American Ceramic Society*, 83:2117–2146, 2000. https://doi.org/10.1111/j.1151-2916.2000.tb01527.x.

[12] A. D. McLachlan. Retarded dispersion forces in dielectrics at finite temperatures. *Proceedings of the Royal Society of London. Series A, Mathematical and Physical Sciences*, 274:80–90, 1963. https://doi.org/10.1098/rspa.1963.0115.

[13] M.H. Hawton, V.V. Paranjape, and J. Mahanty. Temperature dependence of dispersion interaction, application to van der waals forces and the polaron. *Physical Review B*, 26:1682–1688, 1982. https://doi.org/10.1103/physrevb.26.1682.

[14] Rongjia Yang. Is gravity entropic force. *MDPI Entropy*, 16:4483–4488, 2014. https://doi.org/10.3390/e16084483.

[15] Takashi Torii. Violation of the third law of black hole thermodynamics in higher curvature gravity. *MDPI Entropy*, 14:2291–2301, 2012. https://doi.org/10.3390/e14122456.

[16] Oyvind Gron. Entropy and gravity. *MDPI Entropy*, 14:2456–2477, 2012. https://doi.org/10.3390/e14122456.

[17] Jeroen Schoenmaker. Historical and physical account on entropy and perspectives on the second law of thermodynamics for astrophysical and cosmological systems. *MDPI Entropy*, 16:4430–4442, 2014. https://doi.org/10.3390/e16084420.

[18] Alessandro Pesci. Entropy bounds and field equations. *MDPI Entropy*, 17:5799–5810, 2015. https://doi.org/10.3390/e17085799.

[19] Er Shi, Xiaoqin Sun, Yecong He, and Changwei Jiang. Effect of a magnetic quadrupole field on entropy generation in thermomagnetic convection of paramagnetic fluid with and without a gravitational field. *MDPI Entropy*, 19:96, 2017. https://doi.org/10.3390/e19030096.

[20] J. Rossnagel, F. Schmidt-Kaler O. Abah, K. Singer, , and E. Lutz. Nanoscale heat engine beyond the carnot limit. *Physical Review Letters*, 112:030602, 22 January 2014. https://doi.org/10.1103/physrevlett.112.030602.

[21] Jan Klaers, Stefan Faelt, Atac Imamoglu, and Emre Togan. Squeezed thermal reservoirs as a resource for a nanomechanical engine beyond the carnot limit. *Physical Review X*, 7:031044, 13 September 2017. https://doi.org/10.1103/physrevx.7.031044.

[22] Nelly Huei Ying Ng, Mischa Prebin Woods, and Stephanie Wehner. Surpassing the carnot efficiency by extracting imperfect work. *New Journal of Physics*, 19:113005, 7 November 2017. https://doi.org/10.1088/1367-2630/aa8ced.

[23] Otto. Redlich and J. N. S. Kwong. On the thermodynamics of solutions. v. an equation of state. fugacities of gaseous solutions. *Chemical Reviews*, 44(a):233–244, 1949. https://doi.org/10.1021/cr60137a013.

[24] Ding-Yu Peng and Donald B. Robinson. A new two-constant equation of state. *Industrial and Engineering Chemistry Fundamentals*, 75(1):59–64, 1976. https://doi.org/10.1021/i160057a011.

[25] Nathan S. Osborne, Harold F. Stimson, and Defoe C. Ginnings. Measurements of heat capacity and heat of vaporization of water in the range 0 to 100 C. *Part of Journal of Research of the National Bureau of Standards*, 23:197–260, 1939. https://doi.org/10.6028/jres.023.008.

[26] Nathan S. Osborne, Harold F. Stimson, and Defoe C. Ginnings. Thermal properties of saturated water and steam. *Journal of Research of the National Bureau of Standards*, 23:261–270, 1939. https://doi.org/10.6028/jres.023.009.

[27] Reiner Tillner-Roth and Hans Dieter Baehr. An international standard formulation for the thermodynamic properties of 1,1,1,2-tetrafluoroethane (hfc-134a) for temperatures from 170 k to 455 k and pressures up to 70 mpa. *Journal of Physical and Chemical Reference Data*, 23(5):657–729, 1994. https://doi.org/10.1063/1.555958.

[28] Roland Span, Eric W. Lemmon, Richard T Jacobsen, Wolfgang Wagner, and Akimichi Yokozeki. A reference equation of state for the thermodynamic properties of nitrogen for temperatures from 63.151 to 1000 k and pressures to 2200 mpa. *Journal of Physical and Chemical Reference Data*, 29(6):1361–1433, 2000. https://doi.org/10.1063/1.1349047.

[29] W. Wagner and A. Prub. The iapws formulation 1995 for the thermodynamic properties of ordinary water substance for general and scientific use. *Journal of Physical and Chemical Reference Data*, 31(2):387–535, 2002. https://doi.org/10.1063/1.1461829.

[30] U. Setzmann and W. Wagner. A new equation of state and tables of thermodynamic properties for methane covering the range from the melting line to 625 k at pressures up to 100 mpa. *Journal of Physical and Chemical Reference Data*, 20(6):1061–1155, 1991. https://doi.org/10.1063/1.555898.

[31] Daniel G. Friend, Hepburn Ingham, and James F. Fly. Thermophysical properties of ethane. *Journal of Physical and Chemical Reference Data*, 20(2):275–347, 1991. https://doi.org/10.1063/1.555881.

[32] H. Miyamoto and K. Watanabe. A thermodynamic property model for fluid-phase propane. *International Journal of Thermophysics*, 21(5):1045–1072, 2000. https://doi.org/10.1023/a:1026441903474.

[33] H. Miyamoto and K. Watanabe. Thermodynamic property model for fluid-phase n-butane. *International Journal of Thermophysics*, 22(2):459–475, 2001. https://doi.org/10.1023/a:1010722814682.

[34] H. Miyamoto and K. Watanabe. A thermodynamic property model for fluid-phase isobutane. *International Journal of Thermophysics*, 23(2):477–499, 2002. https://doi.org/10.1023/a:1015161519954.

[35] Richard B. Stewart and Richard T. Jacobsen. Thermodynamic properties of argon from the triple point to 1200 k with pressures to 1000 mpa. *Journal of Physical Chemistry Reference Data*, 18(1):639–798, 1989. https://doi.org/10.1063/1.555829.

[36] Ch. Tegeler, R. Span, and W. Wagner. A new equation of state for argon covering the fluid region for temperatures from the melting line to 700 k at pressures up to 1000 mpa. *Journal of Physical Chemistry Reference Data*, 28(3):779–850, 1999. https://doi.org/10.1063/1.556037.

[37] M. A. Anisimov, A. T. Berestov, L. S. Veksler, B. A. Kovalchuk, and V. A. Smirnov. Scaling theory and the equation of state of argon in a wide region around the critical point. *Soviet Physics JETP*, 39(2):359–365, 1974.

[38] Kwan Y Kim. Calorimetric studies on argon and hexafluoro ethane and a generalized correlation of maxima in isobaric heat capacity. *PhD Thesis, Department of Chemical Engineering, University of Michigan*, 1974.

[39] William D. McCain Jr and Waldemar T. Ziegler. The critical temperature, critical pressure, and vapor pressure of argon. *Journal of Chemical and Engineering Data*, 12(2):199–202, 1967. https://doi.org/10.1021/je60033a012.

[40] O. Sifner and J. Klomfar. Thermodynamic properties of xenon from the triple point to 800 k with pressures up to 350 mpa. *Journal of Physical Chemistry Reference Data*, 23(1):63–152, 1994. https://doi.org/10.1063/1.555956.

[41] James A. Beattie, Roland J. Barriault, and James S. Brierley. The compressibility of gaseous xenon. ii. the virial coefficients and potential parameters of xenon. *Journal of Chemical Physics*, 19:1222, 1951. https://doi.org/10.1063/1.1748000.

[42] H. H. Chen, C. C. Lim, and Ronald A. Aziz. The enthalpy of vaporization and internal energy of liquid argon, krypton, and xenon determined from vapor pressures. *Journal of Chemical Thermodynamics*, 7:191–199, 1975. https://doi.org/10.1016/0021-9614(75)90268-2.

[43] Richard T. Jacobsen and Richard B. Stewart. Thermodynamic properties of nitrogen including liquid and vapor phases from 63k to 2000k with pressures to 10,000 bar. *Journal of Physical Chemistry Reference Data*, 2(4):757–922, 1973. https://doi.org/10.1063/1.3253132.

[44] Lester Haar and John S. Gallagher. Thermodynamic properties of ammonia. *Journal of Physical Chemistry Reference Data*, 7(3):635–792, 1978. https://doi.org/10.1063/1.555579.

[45] N. S. Osborne, H. F . Stimson, and D. C. Ginnings. Calorimetric determination of the thermodynamic properties of saturated water in both the liquid and gaseous states from 100 to 374 C. *J. Research NBS*, 18(389):983, 1937.

[46] H. Sato, K. Watanabe, J.M.H Levelt Sengers, J.S. Gallagher, P.G. Hill, J. Straub, and W. Wagner. Sixteen thousand evaluated experimental thermodynamic property data for water and steam. *Journal of Physical Chemistry Reference Data*, 20(5):1023–1044, 1991. https://doi.org/10.1063/1.555894.

[47] Leighton B. Smith and Frederick G. Keyes. The volumes of unit mass of liquid water and their correlation as a function of pressure and temperature. *Procedures of American Academy of Arts and Sciences*, 69:285, 1934. https://doi.org/10.2307/20023049.

[48] D. M. Murphy and T. Koop. Review of the vapor pressures of ice and supercooled water for atmospheric applications. *Q. J. R. Meteorological Society*, 131:1539–1565, 2005. https://doi.org/10.1256/qj.04.94.

[49] B. A. Younglove and J. F. Ely. Thermophysical properties of fluids, methane, ethane, propane, isobutane, and normal butane. *Journal of Physical Chemistry Reference Data*, 16(4):577–798, 1987. https://doi.org/10.1063/1.555785.

[50] Manson Benedict, George B. Webb, and Louis C. Rubin. An empirical equation for thermodynamic properties of light hydrocarbons and their mixtures i. methane, ethane, propane and nbutane. *AIP Journal of Chemical Physics*, 8:334, 1940. https://doi.org/10.1063/1.1750658.

[51] M. Born and H.S. Green. A general kinetic theory of liquids, the molecular distribution functions. *Proceedings of the Royal Society of London Series A Mathematical and Physical Sciences*, 188, 1946. https://doi.org/10.1098/rspa.1946.0093.

[52] G.R. Liu and M.B. Liu. *Smoothed Particle Hydrodynamics: a meshfree particle method*. World Scientific Publishing Co. Pte. Ltd., Suite 202, 1060 Main Street, River Edge NJ 07661, 2003.

[53] W.G. Hoover. *Smooth Particle Applied Mechanics: The State of the Art*. World Scientific Publishing Company, 27 Warren St, Hackensack NJ 07601, 2006.

[54] P.J. Linstrom and Eds W.G. Mallard. *NIST Chemistry WebBook, NIST Standard Reference Database Number 69*. National Institute of Standards and Technology, Gaithersburg MD, 20899, April 29 2018. https://doi.org/10.18434/T4D303.

[55] A.T.A.M. de Waele. Basics of joule–thomson liquefaction and jt cooling. *Springer Journal of Low Temperature Physics*, 186:385–408, 17 January 2017. https://doi.org/10.1007/s10909-016-1733-3.

[56] Roland Span and Wolfgang Wagner. A new equation of state for carbon dioxide covering the fluid region from the triple point temperature to 1100 k at pressures up to 800 mpa. *AIP Journal of Physical and Chemical Reference Data*, 25(6):1509–1596, 15 October 2009. https://doi.org/10.1063/1.555991.

[57] Kenneth S. Pitzer. Phase equilibria and fluid properties in the chemical industry. *American Chemical Society Symposium Series*, 60:1–10, 1977.